Proceedings of the ASME 2019
Dynamic Systems and Control Conference
DSCC 2019
October 8-11, 2019, Park City, UT, USA

DSCC2019-9060

MODELING ACTUATION OF IONOMER CILIA IN SALT SOLUTION UNDER AN EXTERNAL ELECTRIC FIELD

Alain Boldini
Maxwell Rosen
Department of
Mechanical and Aeronautical Engineering
New York University
Tandon School of Engineering
Brooklyn, New York 11201

Youngsu Cha
Center for Intelligent
& Interactive Robotics
Korea Institute of
Science and Technology
Seoul, 02792
Republic of Korea

Maurizio Porfiri *
Department of
Mechanical and Aeronautical Engineering
Department of
Biomedical Engineering
New York University
Tandon School of Engineering
Brooklyn, New York 11201
mporfiri@nyu.edu

ABSTRACT

A recent experiment by Kim's group from the University of Nevada, Las Vegas has demonstrated the possibility of actuating ionomer cilia in salt solution. When these actuators are placed between two external electrodes, across which a small voltage is applied, they move toward the cathode. This is in stark contrast with the case of ionic polymer metal composites, where these ionomers are plated by metal electrodes and bending occurs towards the anode. Here, we seek to unravel the factors underlying the motion of ionomer cilia in salt solution through a physically-based model of actuation. In our model, electrochemistry is described through the Poisson-Nernst-Planck system in terms of concentrations of cations and anions and voltage, which is solved through the finite element method. Based on computer simulations, we establish that Maxwell stress is the main driving force for the motion of the cilia.

INTRODUCTION

The range of applications of ionic polymer metal composites (IPMCs) has been recently expanding due to the new advances in freeform fabrication of ionic membranes [1, 2], which allows for tailoring the performance and geometry of IPMCs. This new class of electroactive materials has been considered for applications as actuators, sensors, and energy harvesters [3–5]. In particular, their large compliance, ability to operate underwater, and small driving voltages have attracted the attention of researchers for underwater biomimetic robotics [6], including robotic fish [7, 8], jelly fish [9, 10], and manta rays [11].

IPMCs are composite materials, comprising a core ionomer layer and two noble metal electrodes on each side [4, 5]. In the ionomer, anions are fixed, while positively charged counterions are mobile. When a voltage is applied across the electrodes of the IPMC, the counterions redistribute through the thickness. Their motion generates differential osmotic pressure and polarization forces, in the form of a Maxwell stress [12], concentrated in boundary layers near the electrodes, where counterions pile-up (anode) or deplete (cathode). These two physical phenomena elicit the macroscopic deformations observed in IPMCs.

Inspired by cilia and flagella in cells, Kim's group from the University of Nevada, Las Vegas recently demonstrated the possibility of actuating ionomer fibers without plated electrodes [13]. When placed between two external electrodes in a salt solution, these actuators show a consistent motion toward the cathode as an electric field is applied across the external electrodes. This configuration allows to overcome difficulties in material processing encountered with standard actuators with electrodes, namely,

*Address all correspondence to this author.

issues with electrode patterning and wiring that complicate manufacturing and control of the actuators.

In this paper, we put forward a modeling framework to describe the actuation of these ionomer fibers. Grounded in physically-based models of electrochemistry, our approach does not require any fictitious constant, but relies only on physical properties of the material. Due to the difference in time scales and the small deformation, the electrochemistry and the mechanical bending are decoupled, whereby the former acts as an input for the latter [14]. The electrochemical model is based on the Poisson-Nernst-Planck (PNP) system [15], which has been widely used for describing electrolytes [16] and ionomer membranes [17]. The field variables of the problem are the cations and anions concentrations, and the voltage. As a result of charge imbalance, internal stresses due to ion mixing and polarization (osmotic pressure and Maxwell stress) are generated inside the ionomer. This model is implemented, in a two-dimensional setting, in the finite element software COMSOL Multiphysics®. From the results of the simulations, we integrate the internal stresses due to ion mixing and polarization to obtain the resulting bending moments. In this way, we demonstrate that Maxwell stress has a predominant role in the actuation.

In the following, we start by illustrating the experimental setup used by Kim's group [13] and summarize their results. Then, we describe the proposed model, illustrating the electrochemical governing equations. We focus on an approximated solution of our problem, which relies on a finite element implementation of the electrochemical model, and we analyze the results of this simulation. Finally, we highlight future directions of research.

EXPERIMENTAL RESULTS FROM [13]

In the preparation for the experiment, ionomer fibers were manufactured through a melt-drawing process from a Nafion precursor, and functionalized to allow counterions exchange. With this technique, it is possible to produce cilia-like actuators with a diameter in the range $25-45\ \mu$m.

These manufactured fibers were used for the experiment. The experimental setup consisted of a tank with a solution of 0.1 M of lithium chloride (LiCl), in which two external graphite electrodes were suspended (Fig. 1). The distance between the two electrodes was 10 mm and their active submerged area was 100 mm^2. The fiber was clamped with a free length of 42 mm and positioned between the two external electrodes. The tip actuator was slightly under the electrodes, so that a laser displacement sensor was used to accurately measure the tip displacement. A small piece of tape, attached to the tip of the fiber, was used to reflect the laser beam, since ionomer fibers are translucent.

A 5 V square-wave $\bar{\psi}$ was applied across the external electrodes. Two frequencies of excitation were tested: 0.1 Hz and 1 Hz. The results of the experiments are summarized in Fig. 2, where the tip displacement of the ionomer fiber is shown for both these frequencies. The direction of the deflection is always toward the instant cathode, which is the opposite of what is typically observed in the initial stage of actuation of IPMCs, before the onset of back-relaxation [5]. A good repeatability of cyclic actuation is observed, suggesting the possibility of using these actuators as biomimetic oscillating cilia.

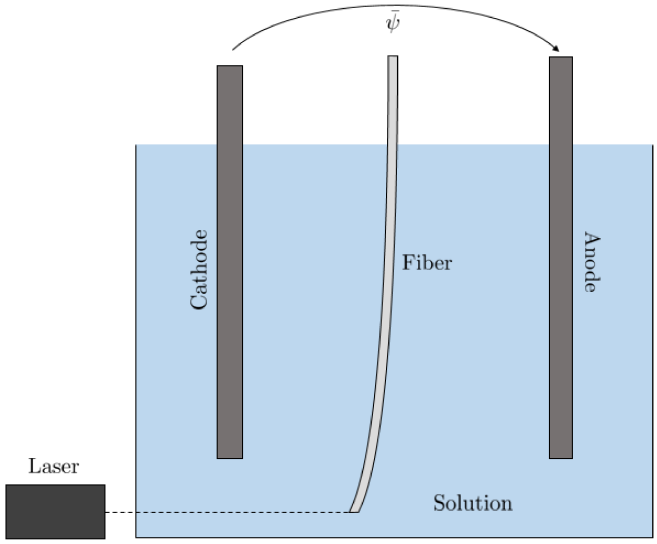

Figure 1. Schematics of the experimental setup by Kim's group [13]. The ionomer fiber is clamped at the top through an external probe. The laser displacement sensor is used to measure the tip displacement of the fiber.

For the 0.1 Hz case, the peak-to-peak tip displacement was about 6 mm, while, for the 1 Hz case, it was around 1 mm. We interpret this difference as the effect of electrolysis of water. In fact, during the initial transient, we expect that the dissociated ions in the solution will be the main current carriers. As time progresses, the dissolved ions should create boundary layers of charge near the electrodes, and the current flow should be related to Faradaic reactions at the electrodes, allowing for a steady-state current. This current is responsible for the continuous increase of tip deflection before the voltage switch for the lower value of the frequency in Fig. 2(a). Its effect is instead reduced by the increased frequency of the square-wave in Fig. 2(b).

As a control condition, the same experiments were performed in deionized water, with a resistivity of 18.2 MΩ cm, indicating minimal, inconsistent response from the fiber.

MODELING FRAMEWORK

In this section, we introduce the framework that is used to model the experiment performed by Kim's group [13]. To simplify our problem, we hypothesize that the deformation has no effect on the electrochemistry. This is motivated by the small

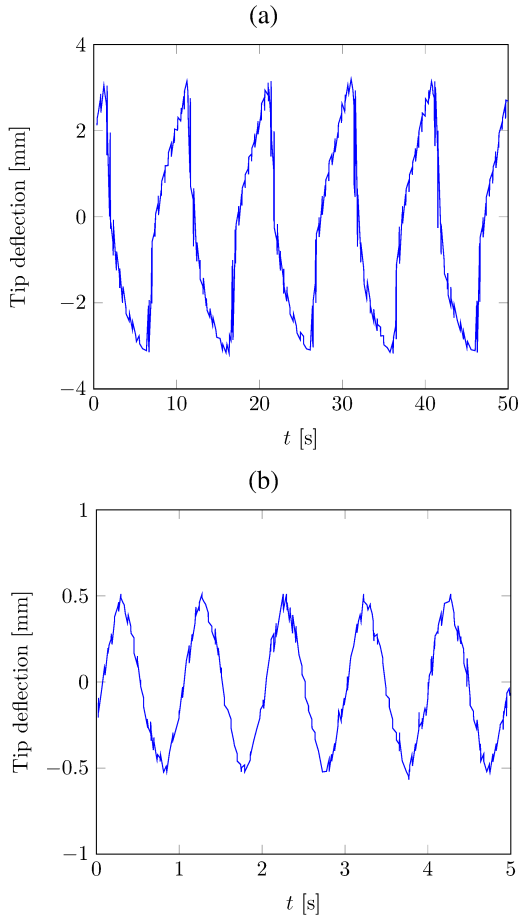

Figure 2. Time trace of the tip displacement of the actuated ionomer fiber for a square-wave voltage of amplitude $\bar{\Psi} = 5$ V applied to the external electrodes. The subplots correspond to a square-wave of frequency 0.1 Hz (a) and 1 Hz (b). The data are reproduced from [13].

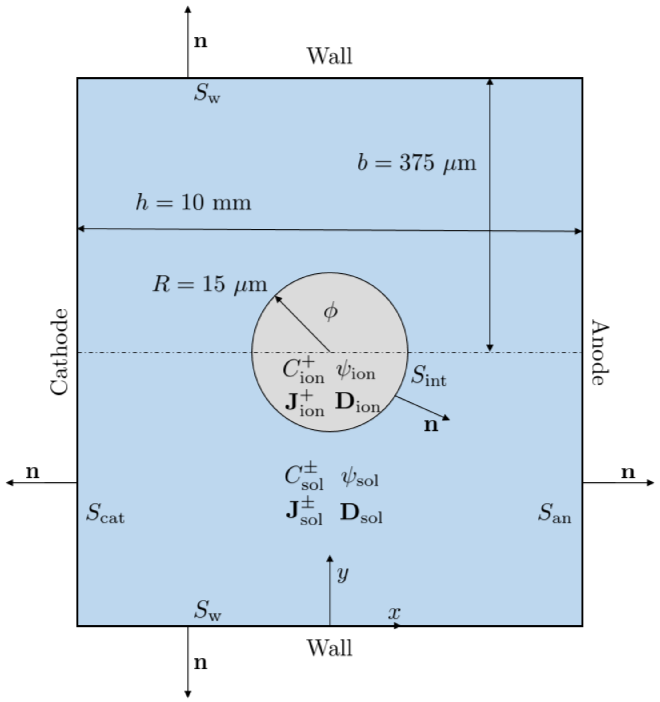

Figure 3. Schematics of the computational domain , with the geometrical parameters used in the simulations. The light blue domain indicates the solution, while the light gray domain represents the ionomer. In each domain, we show the variables defined therein. Each external and internal boundary is indicated by $S_\bullet$, where the subscript is used to discriminate different parts of the boundary. Note that the schematics is not in scale, for illustration purposes.

displacements observed in the experiments conducted by Kim's group [13], and by the separation of the time scales between the electrochemical and mechanical response [14]. Therefore, the electrochemical model is solved on a static domain.

We consider a reference frame with the z-axis aligned with the axis of the actuator, so that the cross-sections lie in planes parallel to the $x-y$ plane, with the x-axis perpendicular to the external electrodes. We neglect three-dimensional effects along the vertical (z) direction, and we focus on a two-dimensional problem on an horizontal cross-section, as shown in Fig. 3.

The electrochemistry is described by the PNP system. Due to the nonlinear form of the electromigration term, closed-form analytical solutions of this system are in general not available for arbitrary geometries and high values of the applied voltage. For this reason, we rely on a numerical solution of the governing equations, as detailed in the following section.

In the solution, mass conservation of positively and negatively charged ions and the Poisson equation are expressed as [16]

$$\frac{\partial C^+}{\partial t} + \nabla \cdot \mathbf{J}^+_{\mathrm{sol}} = 0, \tag{1a}$$

$$\frac{\partial C^-}{\partial t} + \nabla \cdot \mathbf{J}^-_{\mathrm{sol}} = 0, \tag{1b}$$

$$\nabla \cdot \mathbf{D}_{\mathrm{sol}} = Q_{\mathrm{sol}}, \tag{1c}$$

where C^+, C^-, $\mathbf{J}^+_{\mathrm{sol}}$, $\mathbf{J}^-_{\mathrm{sol}}$, $\mathbf{D}_{\mathrm{sol}}$, and Q_{sol} indicate the cations and anions concentrations per unit volume of the solution, the cations and anions fluxes, the electric displacement, and the net charge in the solution, respectively. In addition, $\frac{\partial}{\partial t}(\cdot)$ and $\nabla \cdot (\cdot)$ indicate

the partial derivative with respect to time and the divergence of a vector field.

We assume that the ionic fluxes are governed by the Nernst-Planck equation, modified with a steric coefficient ν which accounts for ion packing at high electric fields [18, 19]. Within this formulation, the concentration of ions in the solution cannot become higher than $\frac{C_{0_{\text{sol}}}}{\nu}$, where $C_{0_{\text{sol}}}$ is the initial concentration in the solution. In addition, we suppose that the solution behaves as a dielectric material, and that there is no Faradaic reaction at the external electrodes. This last assumption is not verified in the experiments by Kim's group [13] as the applied voltage is over the electrolysis standard potential of water; however, we focus on the highest frequency of excitation in [13], that is, 1 Hz, for which we expect the ions in the solution to be the main current carriers. Under these hypotheses, the constitutive equations for the solution are

$$J^+_{\text{sol}} = -\mathcal{D}_{\text{sol}}\left[\nabla C^+ + \frac{\mathcal{F}C^+}{\mathcal{R}\mathcal{T}}\nabla\psi + \frac{\nu C^+}{C_{0_{\text{sol}}} - \nu(C^+ + C^-)}\nabla(C^+ + C^-)\right], \tag{2a}$$

$$J^-_{\text{sol}} = -\mathcal{D}_{\text{sol}}\left[\nabla C^- - \frac{\mathcal{F}C^-}{\mathcal{R}\mathcal{T}}\nabla\psi + \frac{\nu C^-}{C_{0_{\text{sol}}} - \nu(C^+ + C^-)}\nabla(C^+ + C^-)\right], \tag{2b}$$

$$\mathbf{D}_{\text{sol}} = -\varepsilon_{\text{sol}}\nabla\psi, \tag{2c}$$

$$Q_{\text{sol}} = \mathcal{F}(C^+ - C^-). \tag{2d}$$

Here, ψ is the electric potential, $\mathcal{D}_{\text{sol}}$ indicates the diffusivity of ions in solution, assumed to be equal for cations and anions, while $\mathcal{F}$, $\mathcal{R}$, and $\mathcal{T}$ are the Faraday constant, the universal gas constant, and the absolute temperature, respectively. Additionally, $\nabla(\cdot)$ represents the gradient of a scalar field.

In the ionomer, the anions are fixed, and therefore their concentration does not vary in time. We assume that the concentration of anions is also uniform, such that $C^- = C_{0_{\text{ion}}}$ is a constant. Under this hypothesis, the PNP system for the ionomer reduces to [17]

$$\frac{\partial C^+}{\partial t} + \nabla\cdot\mathbf{J}^+_{\text{ion}} = 0, \tag{3a}$$

$$\nabla\cdot\mathbf{D}_{\text{ion}} = Q_{\text{ion}}. \tag{3b}$$

Note that C^+, in this case, is the concentration per total volume of the ionomer. As we expect the concentration of counterions not to grow, we neglect steric effects in the ionomer. By supposing that the ionomer also behaves as a dielectric material, and considering that anions are fixed, we obtain the following constitutive laws:

$$\mathbf{J}^+_{\text{ion}} = -\mathcal{D}_{\text{ion}}\left(\nabla C^+ + \frac{\mathcal{F}C^+}{\mathcal{R}\mathcal{T}}\nabla\psi\right), \tag{4a}$$

$$\mathbf{D}_{\text{ion}} = -\varepsilon_{\text{ion}}\nabla\psi, \tag{4b}$$

$$Q_{\text{ion}} = \mathcal{F}(C^+ - C_{0_{\text{ion}}}), \tag{4c}$$

where we acknowledge that the diffusivity $\mathcal{D}_{\text{ion}}$ and the dielectric constant ε_{ion} of the ionomer can be different than the ones of the solution.

Regarding boundary conditions, at the anode (S_{an}) and at the cathode (S_{cat}) we impose a time-varying voltage

$$\psi_{\text{sol}}|_{S_{\text{cat}}} = -\frac{\bar{\Psi}}{2}(t), \tag{5a}$$

$$\psi_{\text{sol}}|_{S_{\text{an}}} = \frac{\bar{\Psi}}{2}(t). \tag{5b}$$

In such a way, we neglect the effect of the potential drop across the Stern layer [16], simplifying the problem. On the lateral walls, instead, we require that the normal component of the electric displacement is zero, that is,

$$\mathbf{D}_{\text{sol}}\cdot\mathbf{n}|_{S_{\text{w}}} = 0. \tag{6}$$

This boundary condition implies that charges do not accumulate close to the lateral walls, which is a reasonable approximation in the setup of [13]. In addition, we set the ionic fluxes to zero on all the boundaries, consistently with our hypothesis of no Faradaic reactions, through the following conditions:

$$\mathbf{J}^\pm\cdot\mathbf{n}\big|_{S_{\text{cat}}} = \mathbf{J}^\pm\cdot\mathbf{n}\big|_{S_{\text{an}}} = \mathbf{J}^\pm\cdot\mathbf{n}\big|_{S_{\text{w}}} = 0. \tag{7}$$

To close the problem, matching conditions at the interface S between the ionomer and the solution are imposed. We require that the concentration and flux of counterions are matched

per unit volume of water, whereby we rescale the values in the ionomer by its porosity ϕ, estimated from [20],

$$C^+_{\text{sol}}\big|_{S_{\text{int}}} = \left.\frac{C^+_{\text{ion}}}{\phi}\right|_{S_{\text{int}}}, \tag{8a}$$

$$\mathbf{J}^+_{\text{sol}}\cdot\mathbf{n}\big|_{S_{\text{int}}} = \left.\frac{\mathbf{J}^+_{\text{ion}}}{\phi}\cdot\mathbf{n}\right|_{S_{\text{int}}}. \tag{8b}$$

As the ionomer is selectively permeable, we require that the flux of anions is zero at the interface

$$\mathbf{J}^-_{\text{sol}}\cdot\mathbf{n}\big|_{S_{\text{int}}} = 0. \tag{9}$$

Finally, we match the values of the electric potential and the normal component of the electric displacement across the interface

$$\psi_{\text{sol}}\big|_{S_{\text{int}}} = \psi_{\text{ion}}\big|_{S_{\text{int}}}, \tag{10a}$$

$$\mathbf{D}_{\text{sol}}\cdot\mathbf{n}\big|_{S_{\text{int}}} = \mathbf{D}_{\text{ion}}\cdot\mathbf{n}\big|_{S_{\text{int}}}. \tag{10b}$$

The latter condition ensures that no surface charge is generated at the interface.

The actuator is considered as a beam forced by osmotic pressure and Maxwell stress, which generate two internal bending moments M_{ionic} and M_{pol}, respectively, given by

$$M_{\text{ionic}} = -\mathcal{R}\mathcal{T}\int_{\Omega_{\text{ion}}}(C^+ - C_0)x\,\mathrm{d}\Omega_{\text{ion}}, \tag{11a}$$

$$M_{\text{pol}} = \frac{\varepsilon_{\text{ion}}}{2}\int_{\Omega_{\text{ion}}}\|\mathbf{E}\|^2 x\,\mathrm{d}\Omega_{\text{ion}}, \tag{11b}$$

where $\mathbf{E} = -\nabla\psi$ is the electric field, $\|\cdot\|$ indicates the norm of a vector field, and Ω_{ion} is the two-dimensional domain occupied by the ionomer.

FINITE ELEMENT SOLUTION

We now present a numerical solution of the proposed model. In particular, we solve the electrochemical problem in the commercial finite element software COMSOL Multiphysics®.

We exploit the symmetry with respect to the vertical plane perpendicular to the electrodes and passing through the middle of the cylinder to simulate only half of the domain, as shown in Fig. 4, reducing the computational cost. The presence of thin boundary layers at the electrodes and at the interface between the ionomer and the solution, in fact, requires very fine meshes (as evidenced from Fig. 4), implying expensive and ill-conditioned computations. In addition, we decrease the dimension of the domain by reducing the width of the electrodes, while assuring that no interaction between the wall and the ionomer takes place.

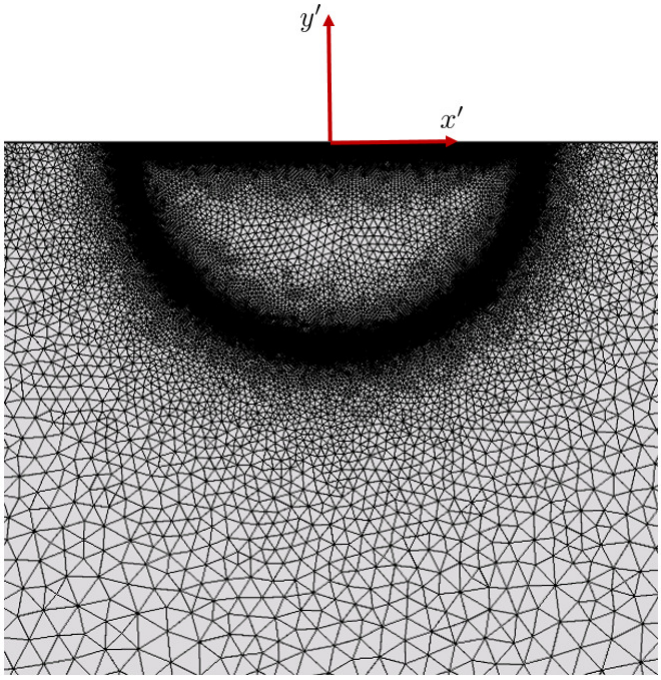

Figure 4. Detailed view of the mesh used in the simulations, highlighting the refining of the mesh near the interface between the ionomer and the solution to properly capture boundary layers. Axes x' and y' are parallel to x and y axes in Figure 3, respectively.

In our simulations, we do not seek for quantitative agreement with experiments, as we do not have access to the unknown material parameters, but we try to obtain some qualitative information about the physics of the problem. Therefore, to enhance the convergence of the simulation, we substitute the 5 V square-wave from the experiment of Kim's group [13] with a sinusoidal input of the same amplitude and frequency. This choice yields reduced values of the bending moments. Furthermore, we use a slightly higher value of the dielectric constant of Nafion membranes in salt solution than the one measured in literature [21], further reducing the computational cost by increasing the thick-

ness of the boundary layers. The dielectric constant of the water is multiplied by the same factor to maintain the same ratio between the two dielectric constants. The parameters used in the simulations are listed in Table 1.

Table 1. Model parameters.

Parameter	Value
$\mathcal{T}$ [K]	300
C_0 [mol m^{-3}]	1070
C_{0_s} [mol m^{-3}]	100
$\mathcal{D}_i$ [m^2 s^{-1}]	3.84×10^{-10}
$\mathcal{D}_s$ [m^2 s^{-1}]	1×10^{-9}
ε_i [F m^{-1}]	8.854×10^{-7}
ε_s [F m^{-1}]	7.083×10^{-9}
ϕ	0.3837
ν	0.0033

At the beginning of the simulation, the steady-state solution for no external electric field applied is found. In fact, the counterions of the ionomer near the interface diffuse into the solution, to establish electrochemical equilibrium [22]. With the steady-state condition as the initial state of our system, we simulate the response over a half period to evaluate the time-varying internal bending moments in the membrane.

The time steps in the COMSOL Multiphysics® simulation are advanced through a backward differentiation formula (BDF). The standard multifrontal massively parallel sparse direct solver (MUMPS) implemented in COMSOL is used for the solution of the sparse systems generated by finite elements.

RESULTS

Figure 5 shows the evolution in time of the bending moments due to ion mixing and polarization, computed from our simulation. Interestingly, we find that the contribution of Maxwell stress is predominant over osmotic pressure. This observation is consistent with the actuators' deflection toward the cathode, such as during back-relaxation in IPMCs [23]. In one of our previous work [24], we proposed an alternative explanation of back-relaxation in IPMCs, in which Maxwell stress is responsible for the final relaxation toward the cathode.

A possible explanation regarding the onset of a considerable Maxwell stress is given in Fig. 6, where we show the ions concentration colormaps in the solution for the peak response time in

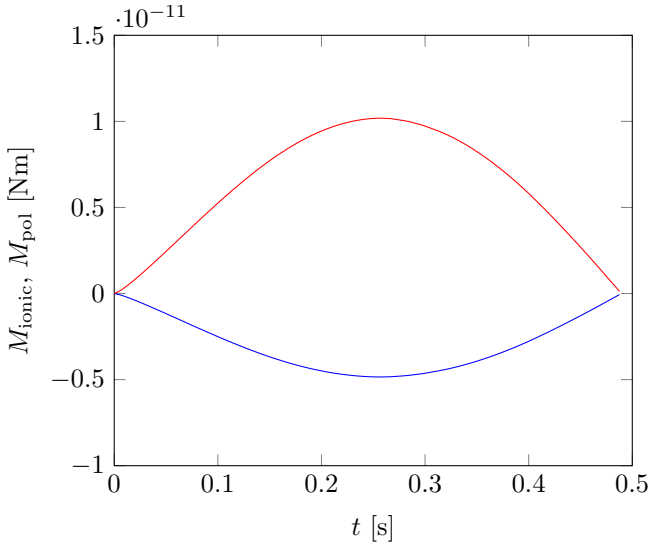

Figure 5. Time evolution of the bending moment due to ion mixing (blue) and related to Maxwell stress (red) over a half period for a sinusoidal input voltage $\bar{\Psi}(t)$ with amplitude 5 V and frequency 1 Hz.

Fig. 5. While charges tend to pile-up on the side facing the cathode, a considerable depletion is observed on the opposite side. This depletion of charges may be responsible for the generation of relatively high intensity electric fields [25], which explains the dominance of Maxwell stress.

In Fig. 7, we display an arrow surface plot of the gradient of the electric potential ($-\mathbf{E}$), for the time at which the voltage reaches its peak value. We observe that the electric field near the interface is much larger than the electric field in the bulk of the solution, and has a radial direction. No considerable electric field is found in the bulk of the ionomer.

Consistently with the sign of the bending moment related to polarization in Fig. 5, we find that the electric field is higher on the side of the ionomer facing the anode. Consequently, Maxwell stress is larger on that side of the actuator, eliciting a net bending moment toward the cathode. This difference has to be traced back to the charge imbalance inferred from Fig. 6, which is dissimilar on the two sides of the ionomer cilia. The ultimate explanation of this behavior is the selective permeability of the ionomer, which allows charge pile-up and depletion on its two sides, limited by two-dimensional transport phenomena.

To additionally substantiate our claims, we plot in Fig. 8 the nondimensional electric field over the surface of the cilia for two time instants, that is, the initial condition and the time for which the applied voltage is maximum. While showing a clear trend, the data display high frequency noise, likely related to numerical issues in the numerical evaluation of the gradient of the potential near the interface. In particular, three factors may contribute to this issue: the high density of the mesh near the interface, the

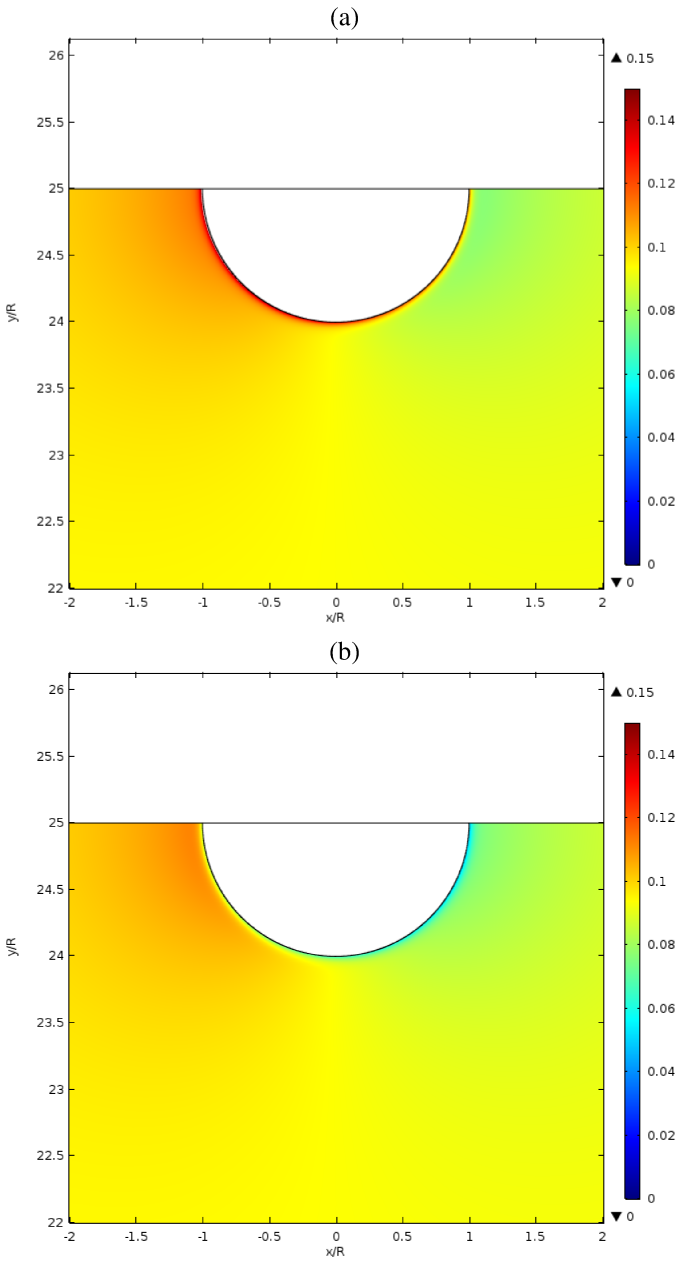

Figure 6. Colormaps of the concentrations of cations (a) and anions (b) in the solution for $t = 0.25$ s. The scale on the right indicates the ratio between the actual concentration and the concentration of the anions in the ionomer.

error in defining the curved surface of the cilia for the discretization introduced by mesh triangulation, and the presence of steep boundary layers.

For the initial condition, we find a non-zero electric field, due to counterions migration and formation of a Donnan potential in the bulk of the ionomer, which is lower than the potential in the solution [22]. However, the value of the electric field is uniform over all the surface, and a zero net bending moment is generated.

At the time in which the voltage reaches its peak value, instead, the distribution of the electric field is anti-symmetric. Consistent with Fig. 7, we observe a decrease in the norm of the electric field on the side of the ionomer facing the cathode (0 to $\frac{\pi}{2}$), and an increase on the anode side ($\frac{\pi}{2}$ to π), while the electric field for the point equidistant from the two electrodes is approximately equal to the electric field at the initial time. This symmetry break elicits a net bending moment due to Maxwell stress, which we recognize as the main driving phenomenon of the ionomer motion.

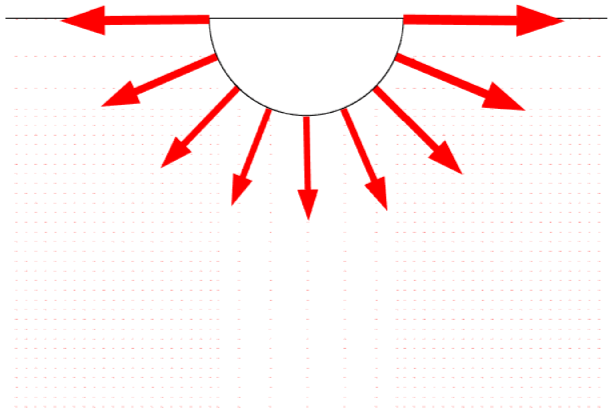

Figure 7. Arrow surface representing the gradient of the electric potential in the vicinity of the ionomer cilia for $t = 0.25$ s.

CONCLUSION

Here, we have proposed a model to describe the actuation of ionomer fibers immersed in salt solution and subjected to an external electric field. In this model, electrochemistry, decoupled from the deformation, is solved through finite element simulations, from which the internal bending moments due to ion mixing and polarization are computed. We observe that the contribution related to Maxwell stress prevails over the one due to osmotic pressure. The results of this work can inform the design of ionomer cilia-like actuators for biomimetic applications. Future endeavors will include a thorough study of the mechanism of

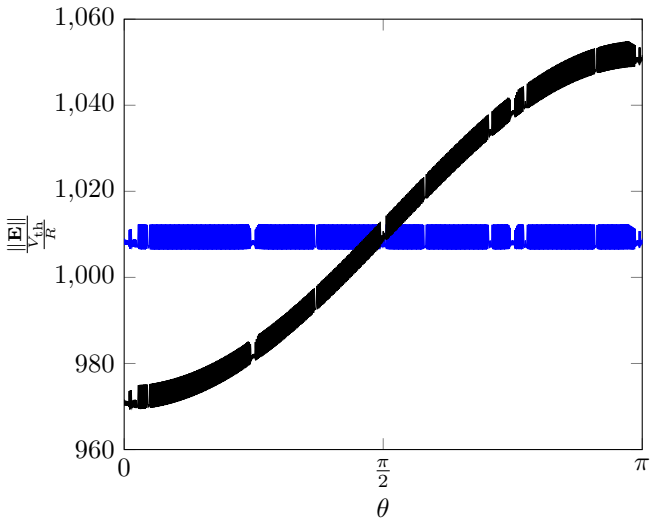

Figure 8. Nondimensional electric field over the surface of the ionomer for the initial condition (blue) and at $t = 0.25$ s (black). θ indicates the angle between the point on the surface and the perpendicular to the cathode, considered 0 at the nearest point to the cathode and π on the opposite point. The electric field is nondimensionalized with $\frac{V_{th}}{R}$, where $V_{th} = \frac{\mathcal{R}\mathcal{T}}{\mathcal{F}}$ is the thermal voltage and R is the radius of the cilia.

actuation of ionomer fibers through Maxwell stress, with further controlled experimental conditions.

ACKNOWLEDGMENT

This research was supported by the National Science Foundation under Grant No. OISE-1545857 and by KIST flagship program under Project No. 2E29460.

REFERENCES

[1] Carrico, J. D., Tyler, T., and Leang, K. K., 2017. "A comprehensive review of select smart polymeric and gel actuators for soft mechatronics and robotics applications: fundamentals, freeform fabrication, and motion control". *International Journal of Smart and Nano Materials,* **8**(4), pp. 144–213.

[2] Stalbaum, T., Trabia, S., Hwang, T., Olsen, Z., Nelson, S., Shen, Q., Lee, D.-C., Kim, K. J., Carrico, J., Leang, K. K., Palmre, V., Nam, J., Park, I., Tiwari, R., Kim, D., and Kim, S., 2018. "Guidelines for making ionic polymer-metal composite (IPMC) materials as artificial muscles by advanced manufacturing methods". In *Advances in Manufacturing and Processing of Materials and Structures*, Y. Bar-Cohen, ed. CRC Press, ch. 15.

[3] Bhandari, B., Lee, G.-Y., and Ahn, S.-H., 2012. "A review on IPMC material as actuators and sensors: Fabrications, characteristics and applications". *International Journal of Precision Engineering and Manufacturing,* **13**(1), pp. 141–163.

[4] Jo, C., Pugal, D., Oh, I.-K., Kim, K. J., and Asaka, K., 2013. "Recent advances in ionic polymer-metal composite actuators and their modeling and applications". *Progress in Polymer Science,* **38**(7), pp. 1037–1066.

[5] Shahinpoor, M., ed., 2015. *Ionic Polymer Metal Composites (IPMCs): Smart Multi-Functional Materials and Artificial Muscles*. Smart Materials Series. Royal Society of Chemistry.

[6] Chen, Z., 2017. "A review on robotic fish enabled by ionic polymer-metal composite artificial muscles". *Robotics and Biomimetics,* **4**(24).

[7] Aureli, M., Kopman, V., and Porfiri, M., 2010. "Free-locomotion of underwater vehicles actuated by ionic polymer metal composites". *IEEE/ASME Transactions on Mechatronics,* **15**(4), pp. 603–614.

[8] Chen, Z., Shatara, S., and Tan, X., 2009. "Modeling of biomimetic robotic fish propelled by an ionic polymer-metal composite caudal fin". *IEEE/ASME Transactions on Mechatronics,* **15**(3), pp. 448–459.

[9] Yeom, S.-W., and Oh, I.-K., 2009. "A biomimetic jellyfish robot based on ionic polymer metal composite actuators". *Smart Materials and Structures,* **18**(8).

[10] Najem, J., Sarles, S. A., Akle, B., and Leo, D. J., 2012. "Biomimetic jellyfish-inspired underwater vehicle actuated by ionic polymer metal composite actuators". *Smart Materials and Structures,* **21**(9).

[11] Chen, Z., Um, T. I., and Bart-Smith, H., 2012. "Bio-inspired robotic manta ray powered by ionic polymer-metal composite artificial muscles". *International Journal of Smart and Nano Materials,* **3**(4), pp. 296–308.

[12] Cha, Y., and Porfiri, M., 2014. "Mechanics and electrochemistry of ionic polymer metal composites". *Journal of the Mechanics and Physics of Solids,* **71**, pp. 156–178.

[13] Kim, K. J., Palmre, V., Stalbaum, T., Hwang, T., Shen, Q., and Trabia, S., 2016. "Promising developments in marine applications with artificial muscles: Electrodeless artificial cilia microfibers". *Marine Technology Society,* **50**(5), pp. 24–34.

[14] Porfiri, M., Sharghi, H., and Zhang, P., 2018. "Modeling back-relaxation in ionic polymer metal composites: The role of steric effects and composite layers". *Journal of Applied Physics,* **123**(014901).

[15] Bard, A. J., and Faulkner, L. R., 2001. *Electrochemical Methods - Fundamentals and Applications*. John Wiley & Sons.

[16] Bazant, M. Z., Thornton, K., and Ajdari, A., 2004. "Diffuse-charge dynamics in electrochemical systems". *Physical Review E,* **70**(021506).

[17] Porfiri, M., 2008. "Charge dynamics in ionic polymer metal

composites". *Journal of Applied Physics,* **104**(10).
[18] Kilic, M. S., Bazant, M. Z., and Ajdari, A., 2007. "Steric effects in the dynamics of electrolytes at large applied voltages. I. Double-layer charging". *Physical Review E,* **75**(2).
[19] Kilic, M. S., Bazant, M. Z., and Ajdari, A., 2007. "Steric effects in the dynamics of electrolytes at large applied voltages. II. Modified Poisson-Nernst-Planck equations". *Physical Review E,* **75**(2).
[20] Nemat-Nasser, S., and Li, J. Y., 2000. "Electromechanical response of ionic polymer-metal composites". *Journal of Applied Physics,* **87**(7).
[21] Mauritz, K. A., and Fu, R.-M., 1988. "Dielectric relaxation studies of ion motions in electrolyte-containing perfluorosulfonate ionomers. 1. NaOH and NaCl systems". *Macromolecules,* **21**, pp. 1324–1333.
[22] Moya, A. A., 2015. "Theory of the formation of the electric double layer at the ion exchange membrane-solution interface". *Physical Chemistry Chemical Physics,* **17**, pp. 5207–5218.
[23] Asaka, K., Oguro, K., Nishimura, Y., Mizuhata, M., and Takenaka, H., 1995. "Bending of polyelectrolyte membrane-platinum composites by electric stimuli I. Response characteristics to various waveforms". *Polymer Journal,* **27**, pp. 436–440.
[24] Porfiri, M., Leronni, A., and Bardella, L., 2017. "An alternative explanation of back-relaxation in ionic polymer metal composites". *Extreme Mechanics Letters,* **13**, pp. 78–83.
[25] Chu, K. T., and Bazant, M. Z., 2005. "Electrochemical thin films at and above the classical limiting current". *SIAM Journal of Applied Mathematics,* **65**(5), pp. 1485–1505.